Autofluorescent Granules of the Human Retinal Pigment Epithelium: Phenotypes, Intracellular Distribution, and Age-Related Topography

Katharina Bermond,[1] Christina Wobbe,[1] Ioana-Sandra Tarau,[1] Rainer Heintzmann,[2,3] Jost Hillenkamp,[1] Christine A. Curcio,[4] Kenneth R. Sloan,[4] and Thomas Ach[1]

[1]Department of Ophthalmology, University Hospital Würzburg, Würzburg, Germany
[2]Leibniz Institute of Photonic Technology, Jena, Germany
[3]Institute of Physical Chemistry and Abbe Center of Photonics, Friedrich-Schiller University Jena, Jena, Germany
[4]Department of Ophthalmology, University of Alabama at Birmingham, Birmingham, Alabama, United States

Correspondence: Thomas Ach, Department of Ophthalmology, University Hospital Würzburg, Josef Schneider Strasse 11, 97080 Würzburg, Germany; thomas.ach@ukbonn.de.

Received: January 18, 2020
Accepted: April 9, 2020
Published: May 20, 2020

Citation: Bermond K, Wobbe C, Tarau I-S, et al. Autofluorescent granules of the human retinal pigment epithelium: phenotypes, intracellular distribution, and age-related topography. *Invest Ophthalmol Vis Sci.* 2020;61(5):35. https://doi.org/10.1167/iovs.61.5.35

Purpose. The human retinal pigment epithelium (RPE) accumulates granules significant for autofluorescence imaging. Knowledge of intracellular accumulation and distribution is limited. Using high-resolution microscopy techniques, we determined the total number of granules per cell, intracellular distribution, and changes related to retinal topography and age.

Methods. RPE cells from the fovea, perifovea, and near-periphery of 15 human RPE flat mounts were imaged using structured illumination microscopy (SIM) and confocal fluorescence microscopy in young (≤51 years, n = 8) and older (>80 years, n = 7) donors. Using custom FIJI plugins, granules were marked with computer assistance, classified based on morphological and autofluorescence properties, and analyzed with regard to intracellular distribution, total number per cell, and granule density.

Results. A total of 193,096 granules in 450 RPE cell bodies were analyzed. Based on autofluorescence properties, size, and composition, the RPE granules exhibited nine different phenotypes (lipofuscin, two; melanolipofuscin, five; melanosomes, two), distinguishable by SIM. Overall, lipofuscin (low at the fovea but increases with eccentricity and age) and melanolipofuscin (equally distributed at all three locations with no age-related changes) were the major granule types. Melanosomes were under-represented due to suboptimal visualization of apical processes in flat mounts.

Conclusions. Low lipofuscin and high melanolipofuscin content within foveal RPE cell bodies and abundant lipofuscin at the perifovea suggest a different genesis, plausibly related to the population of overlying photoreceptors (fovea, cones only; perifovea, highest rod density). This systematic analysis provides further insight into RPE cell and granule physiology and links granule load to cell autofluorescence, providing a subcellular basis for the interpretation of clinical fundus autofluorescence.

Keywords: retinal pigment epithelium, autofluorescence, lipofuscin, melanolipofuscin, melanosome

The retinal pigment epithelium (RPE) is a monolayer of cuboidal cells with strong polarity,[1] embedded between photoreceptors apically and Bruch's membrane (BrM) and the choriocapillaris basolaterally.[2] It has numerous functions in maintaining the homeostasis of the outer retina, including replenishing retinoids; forming the outer blood–retina barrier; secreting growth factors, chemokines, and lipoproteins[3]; and the trans-epithelial transportation of nutrients, water, and metabolic endproducts. Daily phagocytosis of shed photoreceptor outer segments leads to the accumulation of non-degradable inclusion bodies, called lipofuscin, within lysosomes of the RPE cell body.[4–6] Although the exact composition of lipofuscin granules has not been determined, it is well accepted that several *bis*-retinoids in lipofuscin have natural autofluorescence (AF).[7] The AF signal from RPE cells is a major contributor to fundus autofluorescence (FAF),[4,8] a non-invasive clinical imaging technique widely used for the diagnosis and management of retinal diseases.

Histologically, RPE cells exhibit three types of lysosome-related granules: lipofuscin (L), melanolipofuscin (ML), and melanosomes (M). Although L and ML show strong AF during blue light excitation, M absorb visible light and exhibit light-blocking phenomena.[2] It has been suggested, however, that M have AF properties in the red and near-infrared excitation range.[9,10]

In early studies, Streeten[11] and Feeney-Burns et al.[12] demonstrated that intracellular RPE granule distribution is age dependent, with L and ML increasing during aging. The electron microscopy studies by Feeney-Burns et al.[12] could

not report absolute numbers of granules per cell because only cross-sectional profiles and not whole cells were analyzed. Newer technologies such as three-dimensional structural electron microscopy enable the determination of whole cell organelle content and have demonstrated the presence of hundreds of granules in RPE cell bodies.[13] Despite this tremendous granule load, RPE cells still exhibit regular polygonal geometry within an intact monolayer.[14] In contrast, in eyes with age-related macular degeneration (AMD), RPE cells tend to lose AF by changing granule distribution and/or fluorophore composition and basally extruding AF granule aggregates from the cytoplasm.[15–18]

In early efforts to enumerate RPE granules,[12] the locations of cells in relation to the fovea were not specified precisely. Prior studies[19–21] have indicated that RPE granule content follows the topography of photoreceptors, with foveal RPE containing little L and many M and having a low AF signal; cells at roughly 3 mm from the fovea exhibit the highest AF intensities. In evolutionary biology, each species' retinal cell topography is optimized for the topography of the local visual environment.[22] Humans have a high-acuity, cone-only fovea from which rods are absent. Rods appear ~175 µm from the foveal center and increase to an elliptical ring of highest density cresting at 3 to 5 mm.[23] The correspondence of RPE AF and photoreceptor topography was recently replicated with methods that allowed precisely specified digital mapping of cells.[14,23]

Previous studies did not elucidate AF properties of individual examined granules or the total AF signal per cell. Recently, we introduced structured illumination microscopy (SIM) for high-resolution imaging of the RPE and its AF granules.[24,25] SIM surpasses Abbe's resolution limit by superimposing an illumination grid on the specimen and causing moiré patterns from which high-frequency sample information is extracted by postprocessing. SIM simultaneously provides AF information for individual granules and high structural resolution.[25]

It is still unclear how intracellular granule deposition (e.g., absolute number of granules, intracellular localization of granules in large sample sizes) changes with normal aging and in AMD. This knowledge, however, would enhance our understanding of normal and pathologic RPE cell biology in several ways; for example, we would be able to uncover the RPE-specific mechanisms that handle this immense granule load while maintaining proper cell function, and, based on the topography of lipofuscin, we would develop a better understanding of the differences in phagosome and phagolysosome production and processing by RPE in rod-rich (perifovea) and cone-rich (fovea) areas of the macula.

The goal of this study was to three-dimensionally image normal human RPE flat mounts of two different age groups using high-resolution SIM, to characterize granules significant for AF imaging within the RPE cell body, and to determine the intracellular distribution of the granules at well-defined retinal locations. Based on such results, the total AF per cell can be calculated and correlated with intracellular granule load. Understanding AF signal sources at the subcellular level will inform and validate existing and new clinical fundus AF imaging techniques.

Methods

All protocols complied with the Declaration of Helsinki, and the use of human tissue was approved by the institutional review boards of the University of Alabama at Birmingham and the University of Würzburg.

Tissue

Fifteen RPE/BrM flat mounts from 15 Caucasian donors (eight were ≤51 years of age, range 16–51 years; seven were >80 years, range 82–90 years) from our previous study were used for imaging.[14] In brief, tissues were obtained as follows: Globes were collected from the Advancing Sight Network (formerly the Alabama Eye Bank; Birmingham, AL, USA) within 4.2 hours of death, prepared and preserved by immersion in 4% paraformaldehyde/0.1-M PBS, and inspected under a dissection microscope equipped with trans- and epi-illumination to exclude macular or retinal pathologies.[26] The neuroretina and choriocapillaris were removed in a multi-step preparation and imaging process to ensure preservation of the exact foveal position (for details, see Supplementary Fig. S1 in Ach et al.[14]). RPE flat mounts were then imaged at three predefined locations using the regional definitions by Polyak[27] as recently summarized by Quinn et al.[28]: fovea, perifovea (4 mm superior to the fovea), and near-periphery at the superior edge of the RPE flat mount (mean distance from fovea, 7.45 ± 1.0 mm).

Imaging with High-Resolution SIM

A commercially available SIM device (ELYRA-S.1, Carl Zeiss Meditec, Jena, Germany) was used for RPE cell imaging, with an excitation wavelength set at 488 nm and emission light collected between 510 and 750 nm. SIM superimposes an illumination grid pattern (grating pitch, 28 µm; exposure times, 100–150 ms) onto the RPE flat mounts. Images were captured using a 63×, numerical aperture 1.40, plan apochromat oil immersion objective and an iXon 885 EMCCD camera (Andor Technology Ltd., Belfast, Northern Ireland, UK), cooled to –63°C.

The SIM scanning area covered 75.56 × 75.40 µm^2 and captured about 20 to 30 RPE cells per location. The z-stacks of SIM images were acquired from apical RPE (first granules in focus) to basal RPE (last granules out of focus) in 100-nm steps. Each z-stack slab consisted of 15 raw images (five grating positions × three rotations; for details, see Ach et al.[17]). All images underwent postprocessing to extract and reconstruct the high-resolution images (extraction and reconstruction were performed using the Zeiss device's internal software, ZEN 2010). This resulted in significantly improved resolution (about 110 nm lateral) compared to common imaging modalities such as wide-field or confocal microscopy at about 200-nm typical resolution (Supplementary Video).

At each location (fovea, perifovea, and near-periphery), 10 adjacent cells were selected from reconstructed SIM images based on visibility of cell boundaries (tiny gaps between two adjacent cells at the basolateral side, visible during scrolling of the z-stack), good image quality, and intact cell layer. Slabs with no granules (i.e., out of focus) or no visible cell structures were removed before analysis. In three donor eyes (donor ages 36, 82, and 88 years), cell boundaries for the foveal cells were not clearly detectable; therefore, for these three foveas, we selected 10 square areas (169 µm^2) equivalent to an average foveal cell (mean area of all analyzed foveal cells in this study, 167 ± 46 µm^2) for analysis.

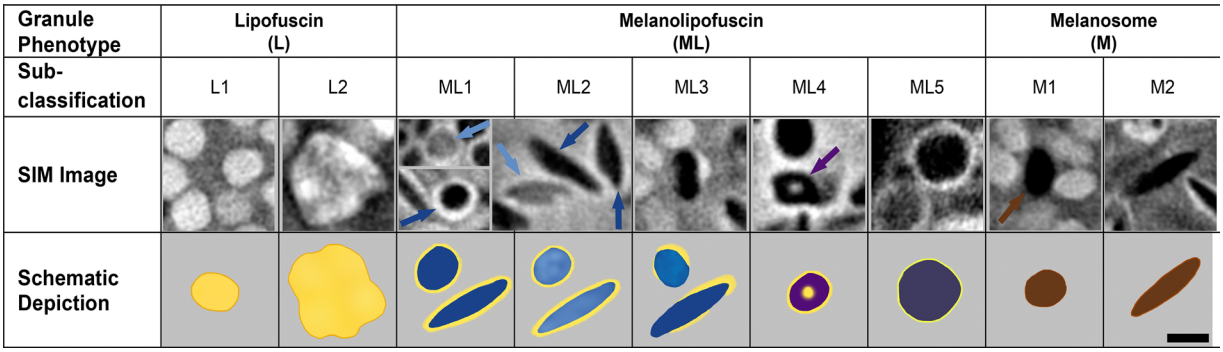

Figure 1. Granule subclassification. Nine different AF granule types were detectable in human RPE cells. For each type an exemplary SIM image and a schematic depiction are shown. For the SIM images, white pixels = high AF intensity and dark pixels = low AF intensity. Iso-AF was defined as the average AF intensity of the cytoplasm of the cell. Lipofuscin L1: round or oval granule exhibiting homogeneous AF; lipofuscin L2: accumulation of compacted inhomogeneous lipofuscin-like AF material larger than L1, with no further delineation of individual granules possible. Note that L2 (multiple lipofuscin-like material) is different from previously described granule aggregates in Ach et al.[17] (accumulations of L1 granule type). Melanolipofuscin ML1: round, oval, or spindle-shaped granules with little to no AF in the center and full AF coating that varies in thickness (light blue - thin coating; dark blue -thick coating); melanolipofuscin ML2: similar to type 1 but with hypo- to iso-AF center; melanolipofuscin ML3: similar to type 1 and 2 but only partly coated with AF material; melanolipofuscin ML4: bull's-eye-shaped granule with AF center surrounded by hypo-AF material and an AF coating; melanolipofuscin ML5: large granule (>2 times L1) with hypo-AF core and weak to distinctive AF coating. Melanosome M1: spherical granule with an absence of both internal AF and AF coating; melanosome M2: spindle-shaped granule with an absence of both internal AF and AF coating. The color coding scheme shown here (L, *yellow*; ML1–3, *blue*; ML4, *violet*; ML5, *dark blue*; M, *brown*) is used for all subsequent figures. *Scale bar*: 1 µm.

SIM Image Preparations and Granule Marking

Using FIJI (https://fiji.sc[29]), a demarcation line was manually drawn with computer assistance around each cell within the reconstructed SIM images (Supplementary Fig. S1), and cell area and height (number of z-stack slabs × 100-nm step size) were reported. A custom FIJI plugin was used for recording granule counts and classifications made by human observers (Supplementary Fig. S1). The code for the plugin (TA_Pick_Particles) is available online (http://sites.imagej.net/CreativeComputation). To further highlight possible differences in intracellular distribution, the SIM stack for each cell was quartered in the *z*-direction into four apical-to-basal quartiles (Q1–Q4), where Q1 to Q3 covered the cushion of granules visible using the SIM technique and Q4 was known to contain abundant non-AF mitochondria.[30,31]

All identifiable granules within the selected RPE cell bodies were manually tagged with computer assistance and independently classified by two trained graders on the basis of granule morphology (see below). For annotation, graders scrolled through the z-stacks and marked the center of each granule with a dot in the slab that revealed the maximum granule dimension. Because individual granules (typical size about 1 µm in diameter[25]) expand over several slabs, previously marked granules were automatically displayed in preceding and subsequent slabs to avoid duplicate assignments (Supplementary Fig. S1). For each tagged granule, the classification code (see below) and its *x*, *y*, *z* coordinates within the stack were registered and written to a text file for further statistical analysis.

Granule Classification

A preliminary analysis of the RPE SIM z-stacks (data not shown) indicated multiple granule subtypes. Based on the AF pattern (AF material at the surface, AF at the core, AF intensity) of each granule and structural properties (spherical vs. spindle shape, size), nine different phenotypes were identified (Fig. 1). These were then used for detailed analysis.

For each cell, the total number of granules per RPE cell body (granules in volumes Q1–Q3) is reported, as it cannot be excluded that preparation artifacts could lead to a loss of apical processes and loss of granules.

Determination of Total Autofluorescence Per Cell

In addition to SIM imaging, RPE flat mounts were imaged at the identical locations (Fig. 2) using a Zeiss LSM 780 laser scanning confocal fluorescence microscope with similar settings: excitation wavelength set at 488 nm and AF emission recorded from 490 to 695 nm in 24 channels (8.9-nm spectral channel width). The scanning area covered 224.92 × 224.92 µm^2, and scans were conducted from apical RPE (first granules in focus) to basal RPE (last granules out of focus) in 390-nm steps, representing the cushion of granules. The laser scanning microscopy (LSM) was performed before SIM imaging, because the bleaching effects of LSM were smaller than those of SIM (z-stack imaging reduced total AF in the imaged area by 0.1% for LSM and 5.1% for SIM, respectively; data not shown).

Using FIJI, within the LSM images, the identical RPE cells as in the SIM images (Fig. 2) were located, marked, and the total AF per cell (AF intensity expressed as a planimetric density) was calculated in two steps: (1) summation of intensities from all pixels of all slabs in the *z*-direction and all spectral channels, resulting in one sum-projected image; and (2) summation of the intensities of all pixels within this image, yielding the total AF intensity of the sum-projected cell.

Statistical Analysis

Nonparametric statistical tests (SPSS Statistics 24 for Mac; IBM, Armonk, NY, USA) were used. For the analysis of non-independent data from the three location groups (i.e., fovea, perifovea, and near-periphery), the Friedman test and post-hoc analysis using Dunn–Bonferroni test were performed. Independent data from two age groups were analyzed using the Mann–Whitney *U* test. A P value < 0.05 was considered

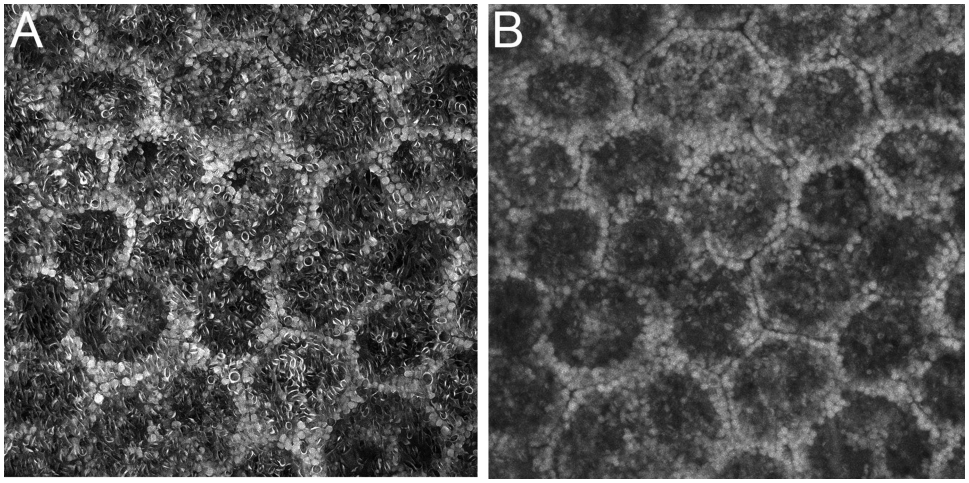

Figure 2. SIM and LSM imaging of RPE cells. At each location, identical RPE cells were imaged using both SIM (**A**) and LSM (**B**). Some lipofuscin granules were pushed toward the basolateral cell borders due to the cell nucleus; however, the relative hypoautofluorescent center of the RPE cells can be attributed to the high content of melanolipofuscin granules and does not exclusively represent the cell nucleus; also see Figure 2 in Starnes et al.[32] The perifovea donor was a 51-year-old female.

significant. The Pearson correlation coefficient was used to measure inter-rater repeatability after classification of granules within 10 cells by the two readers (KB, CW), with a correlation of 0.849 and $P = 0.004$.

Results

Fifteen RPE flat mounts from 15 donor eyes (eight donors ≤ 51 years, seven donors > 80 years) were included. Each flat mount was imaged at three predefined locations (fovea, perifovea, and near-periphery) using SIM and LSM. From these 45 locations, we analyzed 450 cells (30 were square areas of a size mimicking a typical RPE cell, as described in the Methods section).

Introduction of a New Catalog for RPE Granule Subclassification

SIM images revealed a considerable variability of shape, size, and AF pattern of the three major granule types, L, ML, and M. A total of nine granule phenotypes (Fig. 1; Supplementary Table S1) could be defined: L1, uniform L granules; L2, L conglomerates (variable-shaped accumulation of hyper-AF material with irregular intragranular AF patterns, larger than L1); ML1, ML with complete AF coating and minimal AF in the center; ML2, ML with complete AF coating and hypo- to iso-AF in the center; ML3, ML with incomplete AF coating; ML4, bull's-eye-shaped ML with AF coating and AF core; and ML5, large round ML granules with AF coating (greater than twice the volume of a typical L granule). Finally, round (M1) and spindle-shaped (M2) melanosomes could be detected, neither of which showed notable AF components on the surface. Only five granules in the sample could not be classified by this scheme.

During computer-assisted manual grading, it became apparent that uniform L1, bull's-eye-shaped ML4 and large ML5 were clearly distinguishable due to their characteristic appearance (Fig. 1). In contrast, definite differentiation among ML1, ML2, and ML3 was not always possible, due to interchangeable phenotypes, inhomogeneous background AF of the cytoplasm, and sometimes reduced resolution due to screening, mainly by densely packed spindle shaped M or ML. For this reason, results for ML1, ML2, and ML3 granules were pooled (ML1–3).

RPE Cell Area and Granule Content

Dimensions (cell area and equivalent diameter of a circle with the same area) of the selected RPE cells showed comparable results for the ≤51 years versus >80 years age groups (cell area, 202 ± 66 μm^2 vs. 204 ± 76 μm^2; cell diameter, 16 ± 2 μm vs. 16 ± 3 μm). For all donors, foveal cells were distinctly smaller than cells of the perifovea or near-periphery. The cell area (equivalent diameter) for the fovea were 167 ± 46 μm^2 (14 ± 2 μm); for the perifovea, 221 ± 70 μm^2 (17 ± 3 μm); and for the near-periphery, 215 ± 77 μm^2 (16 ± 2 μm) (Fig. 7; Supplementary Table S2).

Within the 450 RPE cells, 193,096 granules were manually marked, counted, and characterized. Overall, the mean number ± standard deviation of granules per cell body was 429 ± 208, with 322 ± 115 at the fovea, 509 ± 198 at the perifovea, and 456 ± 244 at the near-periphery (Fig. 3A; Table). The coefficient of variation for granules per cell at one location was on average between 20% (fovea) and 30% (near-periphery) (Supplementary Table S3).

Interestingly, L dominated at the perifovea and the near-periphery, whereas foveal cell bodies contained only few L granules. The number of L granules per cell body increased significantly with age at all locations (Figs. 3A, 4; Table).

The mean number of overall ML per cell body was comparable for all three locations and showed no age-related changes. ML1–3 were the main granule types at the fovea, and foveal L was low. ML4 and ML5 accounted for only a small proportion of RPE granules, and the mean number of ML4 and ML5 was lowest in foveal cells. ML4 and ML5 showed a significant decrease with age at the fovea and perifovea (Figs. 3A, 3B, 4; Table).

The number of pure M was small; however, comparing numbers from the three examined locations, the highest amount of M was found in foveal cell bodies. M accumula-

Investigative Ophthalmology & Visual Science

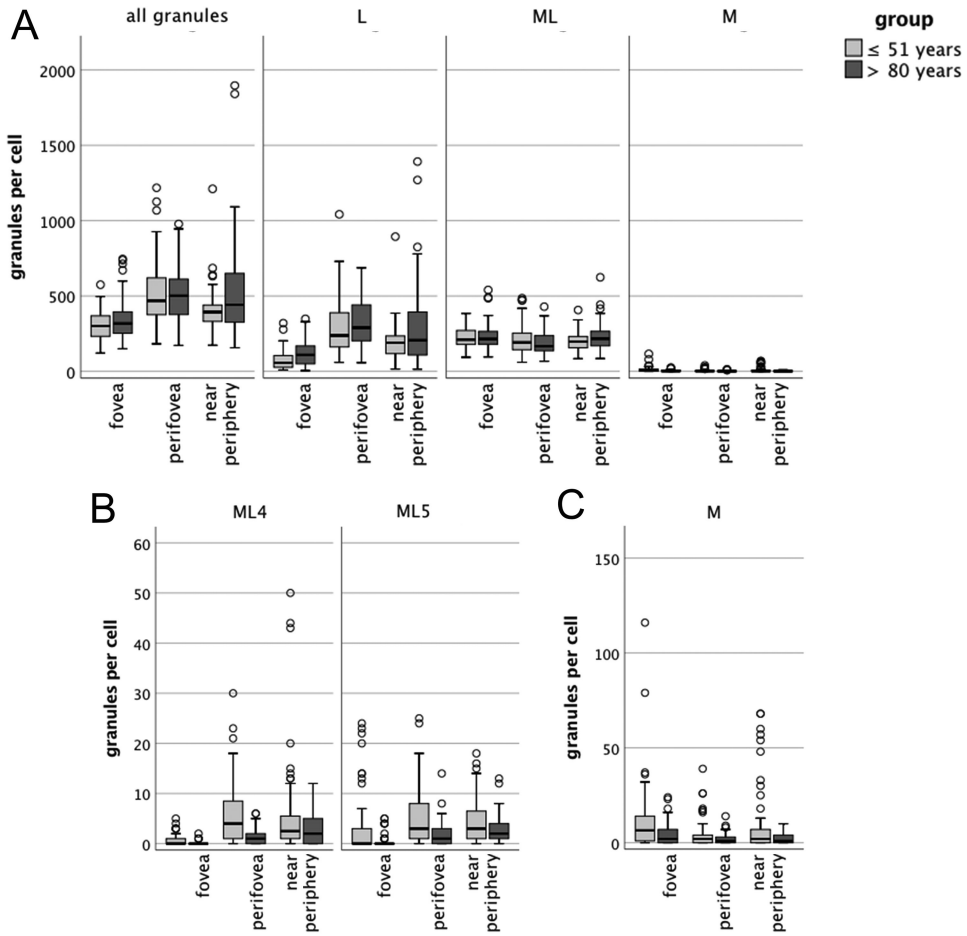

Figure 3. Absolute numbers of granules per RPE cell at the fovea, perifovea, and near-periphery for donor eyes ≤ 51 years and > 80 years. (**A**) RPE cells contain hundreds of granules in their cell bodies, with increasing number at greater age. Foveal RPE cells contained fewer L compared to cells from the other locations. Pure M were found only sporadically, likely due to inconsistent preservation of apical processes in whole mounts. A few large cells containing over 1000 granules were found at the perifovea and near-periphery. (**B**) ML subtypes ML4 and ML5 were low in number and spared the fovea. (**C**) For better illustration, M per cell are plotted with a different scale. The low number of melanosomes might be explained by the possibility of the absence of apical processes (due to preparation artifacts) or the fact that the characterization is based solely on the autofluorescence properties of the granules, meaning that melanosomes that show any kind of autofluorescence at the short wavelengths excitation are counted as melanolipofuscin.

tion showed a significant decrease at all locations with age (Figs. 3A, 3C, 4; Table).

Looking at the specific locations (Figs. 3, 4), the major granule type at the fovea was ML rather than pure L. With greater distance from the fovea, the proportion of intracellular L increased, peaking at the perifovea. With age, the ratio of L to ML shifted to a higher proportion of L. Pure M were barely visible at all locations (Figs. 3, 4), probably due to the loss of apical processes during preparation.[14]

Intracellular Spatial Granule Distribution

RPE cells showed a characteristic intracellular granule distribution (Fig. 5), in both cross-section and en face views. ML were abundant within Q1 to Q3 (cushion of granules visible using SIM autofluorescence), with preferences in the apical Q1 and Q2 of the RPE cell (Fig. 6), whereas L was predominantly located in the basolateral and basal of the RPE cell body (Q2 and Q3 of the RPE cell). The few M granules were found in the apical part of the RPE cell (Q1, Fig. 6). ML4 were located apically (Q1 and Q2), and ML5 were located basally (Q3, Fig. 6). Despite the increasing number of L with increasing age, the overall distribution pattern revealed no significant age-related differences.

RPE Granule Load and Autofluorescence per Cell

To provide a subcellular basis for interpreting clinical FAF, which reduces three-dimensional RPE AF information to a two-dimensional en face projection image, we also looked at granule density (i.e., number of granules per projection area). Overall granule density was highest at the perifovea (2.3 ± 0.5 per μm^2) (Table).

In addition, this analysis revealed that granule load follows cell size (i.e., with increasing number of granules in cells that occupy a larger area) (Fig. 7). At younger ages, the fovea has a narrow range of cell sizes and granule deposition, whereas the perifovea and near-periphery have more variable cell size and granule load. This becomes even more apparent at greater ages, showing more variability in cell size

Investigative Ophthalmology & Visual Science

Table. Number of Granules per Cell or Projection Area at the Fovea, Perifovea, and Near-Periphery

	Number of Granules (Mean ± SD)									
	Per Cell					Per Projection Area				
Granules	Age	Fovea	Perifovea	Near-Periphery	*P*	Age	Fovea	Perifovea	Near-Periphery	*P*
All	≤51 y	307.2 ± 89.3	509.5 ± 201.5	399.2 ± 132.0	<0.001	≤51 y	1.88 ± 0.38	2.26 ± 0.44	1.89 ± 0.38	<0.001
	>80 y	339.1 ± 136,9	508.2 ± 194.4	521.6 ± 316.3	0.001	>80 y	1.98 ± 0.56	2.34 ± 0.55	2.41 ± 0.99	0.001
		$P = 0.271$	$P = 0.815$	$P = 0.017$			$P = 0.331$	$P = 0.342$	$P < 0.001$	
L	≤51 y	73.7 ± 61.0	295.6 ± 181.7	189.0 ± 111.5	<0.001	≤51 y	0.44 ± 0.35	1.27 ± 0.53	0.87 ± 0.35	<0.001
	>80 y	106.3 ± 77.9	317.6 ± 152.1	293.1 ± 260.9	<0.001	>80 y	0.62 ± 0.44	1.45 ± 0.50	1.31 ± 0.86	<0.001
		$P = 0.008$	$P = 0.127$	$P = 0.034$			$P = 0.007$	$P = 0.016$	$P = 0.006$	
ML	≤51 y	223.8 ± 55.9	209.8 ± 86.1	202.1 ± 65.9	<0.001	≤51 y	1.38 ± 0.27	0.97 ± 0.33	0.97 ± 0.32	<0.001
	>80 y	228.4 ± 83.5	188.7 ± 76.4	226.1 ± 88.4	<0.001	>80 y	1.34 ± 0.33	0.88 ± 0.27	1.10 ± 0.37	<0.001
		$P = 0.985$	$P = 0.134$	$P = 0.090$			$P = 0.222$	$P = 0.158$	$P = 0.047$	
M	≤51 y	9.8 ± 17.0	4.1 ± 6.7	8.1 ± 16.0	<0.001	≤51 y	0.06 ± 0.11	0.02 ± 0.04	0.04 ± 0.07	<0.001
	>80 y	4.4 ± 5.4	1.9 ± 2.6	2.3 ± 3.1	<0.001	>80 y	0.02 ± 0.03	0.01 ± 0.01	0.01 ± 0.02	<0.001
		$P = 0.018$	$P = 0.031$	$P = 0.031$			$P = 0.117$	$P = 0.030$	$P = 0.027$	
ML4	≤51 y	0.7 ± 1.3	5.9 ± 6.2	5.4 ± 9.0	<0.001	≤51 y	0.004 ± 0.008	0.028 ± 0.032	0.028 ± 0.049	<0.001
	>80 y	0.1 ± 0.3	1.4 ± 1.6	2.9 ± 2.9	<0.001	>80 y	0.001 ± 0.002	0.006 ± 0.008	0.013 ± 0.014	<0.001
		$P = 0.011$	$P < 0.001$	$P = 0.072$			$P < 0.001$	$P < 0.001$	$P = 0.080$	
ML5	≤51 y	2.6 ± 5.5	5.1 ± 5.4	4.3 ± 4.3	<0.001	≤51 y	0.016 ± 0.035	0.025 ± 0.027	0.020 ± 0.021	<0.001
	>80 y	0.5 ± 1.2	1.8 ± 2.5	2.8 ± 2.9	<0.001	>80 y	0.002 ± 0.006	0.009 ± 0.012	0.013 ± 0.014	<0.001
		$P = 0.047$	$P < 0.001$	$P = 0.067$			$P = 0.001$	$P < 0.001$	$P = 0.063$	

M1 and L2 subtypes were found only sporadically, and those numbers are not presented separately.

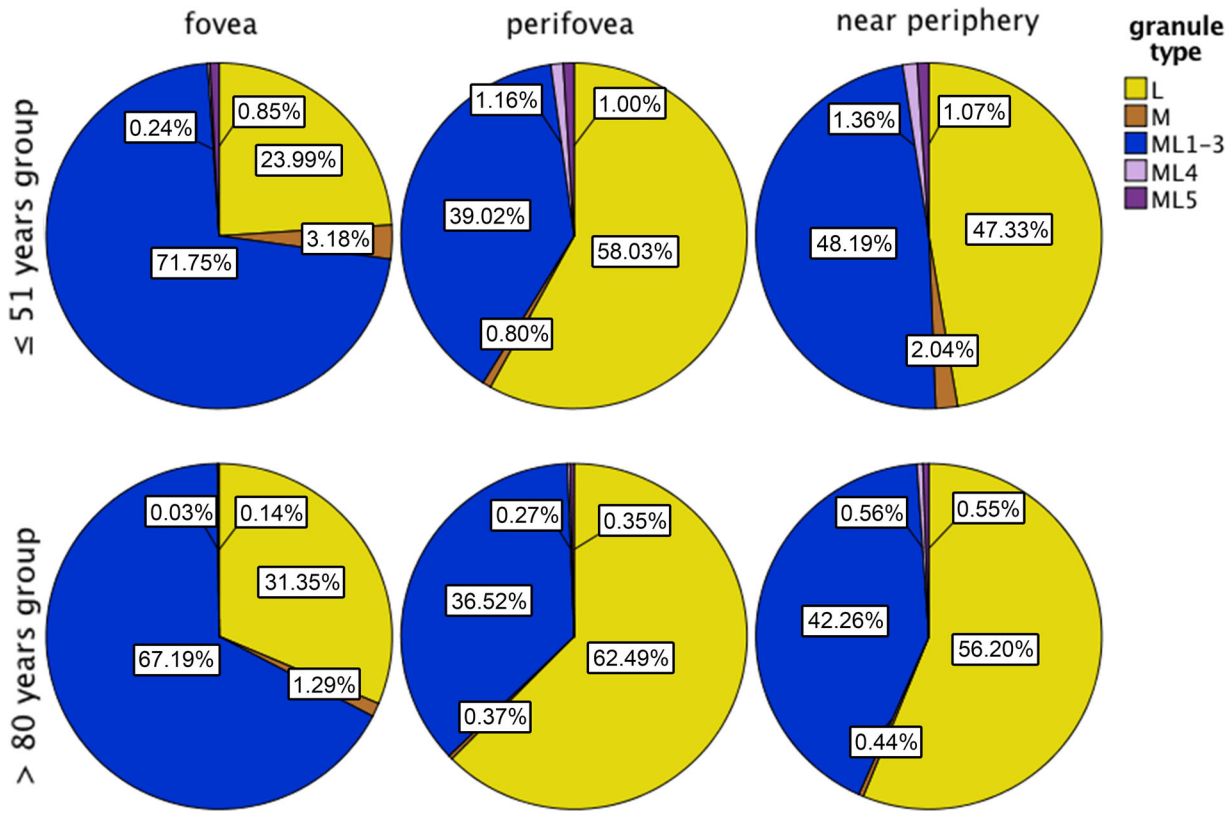

Figure 4. Granule distribution at the fovea, perifovea, and near-periphery. Percentages of L, M, ML1–3, ML4, and ML5 within the RPE cell bodies are plotted. Interestingly, the proportion of pure L was low at the fovea and increased at the perifovea and the near-periphery, peaking at the perifovea. The granule load of RPE cells at the fovea is mainly driven by ML, with ML types ML1–3 being the most abundant. Granules were characterized based on their short-wavelength autofluorescence properties.

Investigative Ophthalmology & Visual Science

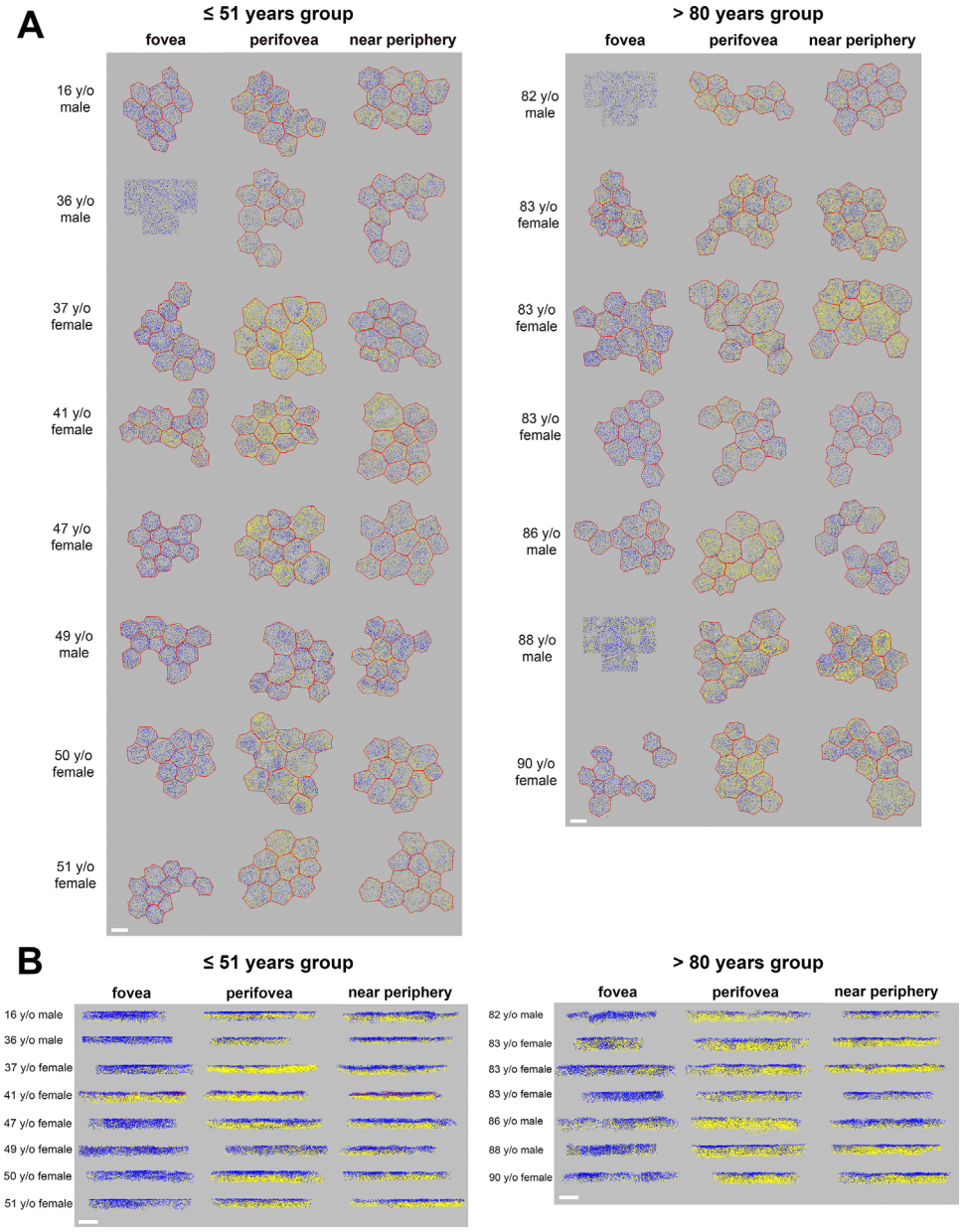

Figure 5. En face and cross-section views of the intracellular granule distribution. (**A**) The en face view shows the high L content in parafoveal and near-peripheral cells, whereas foveal cells contained only a few L. In some cells, L were located more toward cell borders, due to a centrally located nucleus (see also Fig. 2). For three male donors (36, 82, and 88 years old), the cell borders of the foveal cells were not distinguishable in the SIM images. Therefore, 10 square areas equal to the size of a typical foveal RPE cell were analyzed (see Methods). (**B**) ML1–3 was abundant throughout the cushion of organelles of autofluorescent relevance within the RPE cell body (Q1–Q3); however, L was located predominantly at the basolateral and basal parts of the RPE cell bodies (Q2, Q3). With increasing age, the deposition of L increases, especially at the perifovea and near-periphery. The fovea showed only few L granules and many ML granules. Only a few M were seen at the apical side of the RPE cell bodies (Q1). Within the basal parts of the RPE cell bodies (Q4), mitochondria are known to be abundant (not visible in the SIM autofluorescence imaging). Each analyzed granule was color coded and plotted (L, *yellow*; ML1–3, *blue*; ML4, *violet*; ML5, *dark blue*; M, *brown dots*). Because there were only a few M, ML4, and ML5, only a few *violet* or *brown dots* can be spotted. *Red lines* represent cell borders. *Scale bar*: 10 µm.

and number of granules at all locations (Fig. 7, Supplementary Table S2). With an increasing number of granules, the total AF per cell also increased, which was true for the majority of locations. Total AF per cell versus number of granules per cell body did not reveal any aging effects but highlights greater variability in AF at the perifovea and near-periphery as compared with the fovea (Supplementary Fig. S2).

Discussion

This study reports the subcellular microscopy data of more than 193,000 human RPE AF granules. We found that granules within RPE cell bodies exhibit different AF phenotypes and are characteristically deposited intracellularly and in relation to their foveal position. Of note, ML are the major

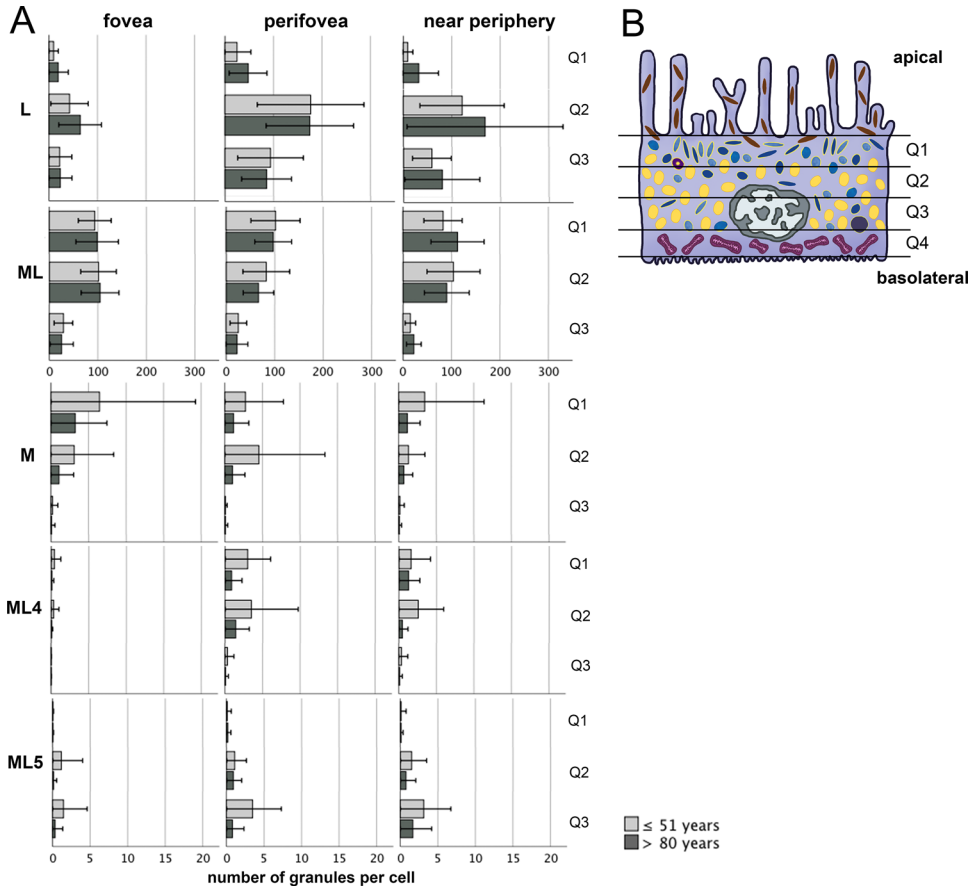

Figure 6. Intracellular granule distribution. (**A**) SIM z-stacks of each cell were divided into three horizontally equally sized parts (upper, middle, and lower). The number of L, ML, M, ML4, and ML5 in each volume is shown. L were found mainly in the middle part, whereas ML, M, and ML4 were most abundant in the upper and middle part and ML5 in the middle and lower part. (**B**) Schematic depiction of an RPE cell (L, *yellow*; ML, *blue*; M, *brown*; nucleus, *gray*; mitochondria, *violet*). Note that the upper and lower scans begin and end with the first and last AF granules in and out of focus, which does not necessarily coincide with the apical and basal ends of the RPE cell.

granule type in RPE cell bodies at the fovea, which underlines clear distinctive phenotypes among RPE bodies related to retinal position and the dominant photoreceptor type in the overlying retina.[32]

Granule Subclassification

High-resolution SIM enables simultaneous high structural resolution and AF imaging of RPE cells,[24,25] which led to our introducing a new granule classification grading system. Based on AF quantity and granule shape, the classic three intracellular RPE granule classes (L, ML, and M)[4] can be further subdivided into nine different phenotypes. A similar classification has been observed using ultrastructural electron microscopy, as recently reported by Pollreisz and colleagues,[13] who described lipofuscin as "a diverse category that may well be subdivided into more granule types." However, electron microscopy (EM) does not reveal AF features of the intracellular granules, and it is not yet clear whether SIM and EM granule classifications are directly interchangeable. For clarification, future studies visualizing the same granules using both techniques (SIM and EM) would be desirable.

In our study, lipofuscin type 1 (L1; 94,203 granules, or 48.8%) represented pure L granules that are primarily located basolaterally within the cushion of autofluorescent granules and prefer perifovea and near-periphery but, interestingly, were found in much lower quantity at the fovea. This reduced accumulation of L at the fovea might reflect specific metabolisms of photoreceptors, especially at the cones-only foveal zone.[23,33] L is thought to be non-degradable material from phagocytosed photoreceptor outer segments,[7] stored in lysosomes within RPE cell bodies. One would expect that at this perfectly specialized area with its high demand for cellular metabolism and strong involvement in visual cycle, RPE cells should show an increased deposition of lipofuscin granules. Determining whether the cone photoreceptor-specific visual cycle[33] at the fovea, which involves Müller cells in addition to RPE cells, leads to less non-degradable material within the RPE cells could be the basis for further studies. However, with greater distance to the fovea, rod photoreceptors outnumber cones by up to 20:1, and the number of L granules within RPE cells increases significantly.

Lipofuscin type 2 (L2) was found only sporadically within the RPE cell bodies (114 out of >193,000 granules, or 0.06%) and revealed properties of a group of encapsulated and more densely packed, but small lipofuscin-like material, compared with the surrounding intracellular L granules. L2 granules were found in both donor age groups but should be distinguished from recently described intracellular RPE granule aggregates,[18] aggregations of multiple L granules

Investigative Ophthalmology & Visual Science

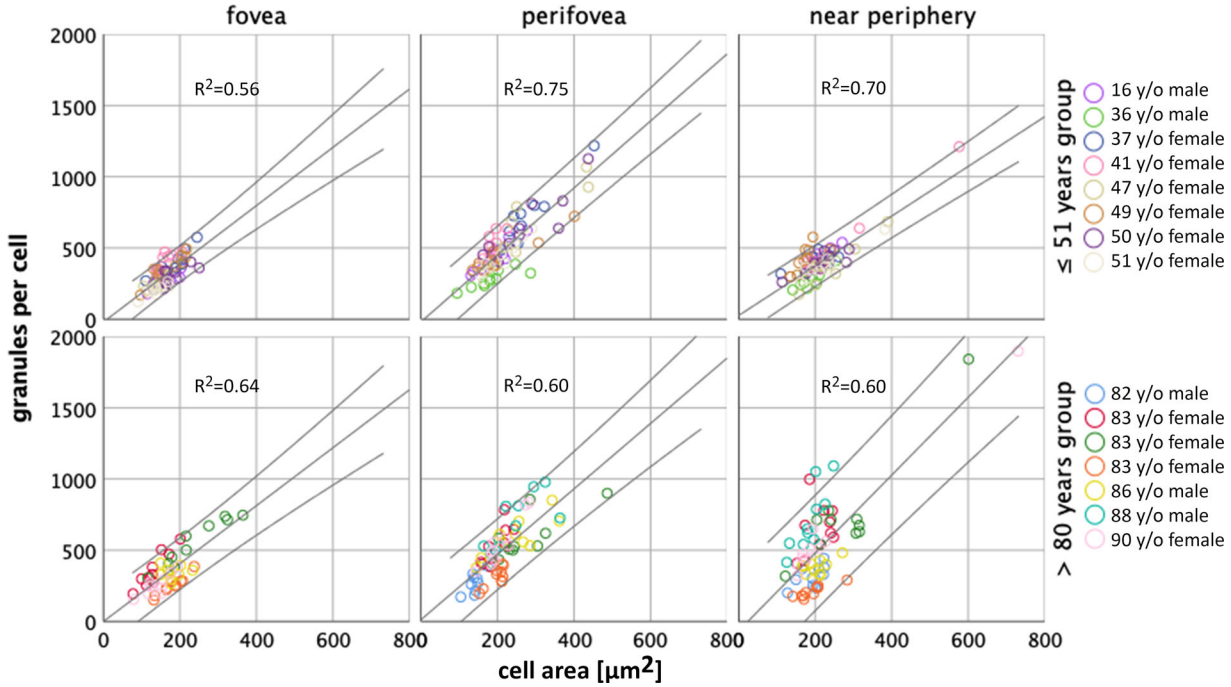

Figure 7. Relationship between cell area and number of granules per cell. Total number of granules per cell increased with larger cell areas for both age groups and at all locations. Foveal cells were smaller (175 ± 53 µm^2) and contained fewer granules in total (322.1 ± 114.7). In general, cells at the perifovea and near -periphery occupied a larger area (perifovea, 225 ± 74 µm^2; near-periphery, 218 ± 73 µm^2), deposited more granules in total (perifovea, 508.9 ± 197.5; near-periphery, 456.3 ± 243.6), and showed a higher variability in granule load than foveal cells. The regression lines and 95% confidence intervals are shown for each location for both age groups.

found almost exclusively in AMD eyes. Granule aggregates are described as a redistribution and compaction of intracellular AF granules that tend to be extruded from the cell body and released into the sub-RPE basal laminar compartment in AMD eyes. In more advanced stages, this loss of granules can lead to decreased AF intensities of RPE cells, as shown for RPE cells in AMD eyes both ex vivo[17] and in vivo.[15,16]

Melanolipofuscin type 4 (ML4; 1271 out of >193,000 granules, or 0.66%) and melanolipofuscin type 5 (ML5; 1314 out of >193,000 granules, or 0.68%) are newly described variants. Both were found almost exclusively outside of the fovea at the apical side (ML4) or basolateral side (ML5), respectively, and presented as ML with an AF core (ML4) or an enlarged ML granule, twice the size of a L granule or even larger (ML5). The number of these granules decreased with age; however, the importance of these granules remains unknown at this point.

Granule Accumulation with Age

As shown in histology from developing and maturating eyes, RPE cells at birth contain melanosomes only.[12,19,20] Several groups have reported AF granules appearing in the first 2 years of life, and only few L granules are found in children under 10 years of age.[19,34] In 1978, Feeney postulated her model of phagocytosis and genesis of AF granules within human RPE cells, showing that AF material is first recognized in RPE phagolysosomes, independent of age.[4]

Feeney suggested that the major source of AF in RPE cells of children under 1 year of age is lipoidal material within secondary lysosomes (melanolysosomes), and that the first L granules appear within the next years in life.[4,12] The immaturity of the fovea at birth[35–37] might explain the absence of lipofuscin granules at this age. As photoreceptor packing density increases in the fovea in the first decade of life,[36,38] non-degradable material and AF lipofuscin granules also increase. At the time of Feeney's study, L accumulation was also thought to be an effect of light exposure.[20] Today, it is well established that the accumulation of AF material depends on rod photoreceptor outer segment all-*trans*-retinal and 11-*cis*-retinal[39] and does not require light,[40] as shown in studies of mouse retina.

However, in Feeney's reports, the exact location of the fovea is missing, and, subsequently, the effect of the characteristic distribution of the overlying photoreceptors on the RPE and L accumulation was not clear.

Based on the AF properties of intracellular granules (Fig. 1), we hypothesized a model of granule accumulation showing transitional states among them (Fig. 8). Melanolipofuscin granules could be intermediate stages between pure melanosomes and lipofuscin granules. Pure melanosomes could merge to form granules with marginal AF material on the surface that might represent early ML stages, leading to ML granules with progressive AF material and, finally, ending up as pure lipofuscin (Fig. 1, granule types ML1 and ML2; Fig. 8). These processes could be explained by the oxidative and/or photooxidative degradation of melanosomes, as shown by in vitro experiments.[41] In contrast, other studies detected different chemical properties of AF material in ML and pure L granules,[42] supporting the idea that L develops de novo intracellularly, independent from the melanin/melanosome pathway. However, developing L granules (i.e., only a few hundred nanometers in size) have not been described so far, and final L size (about 1 µm) does match the pure spherical M size.

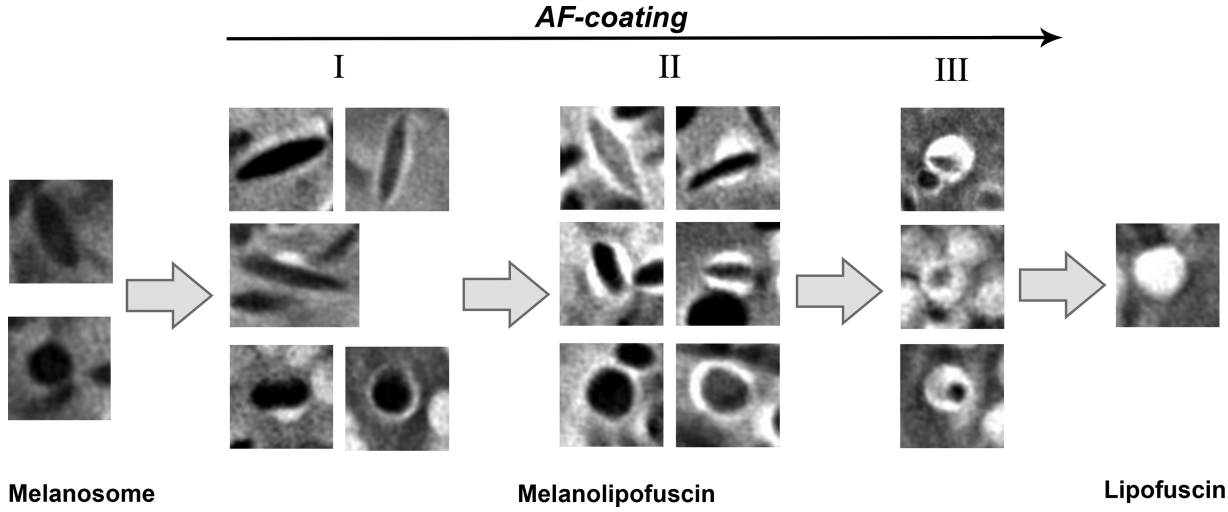

Figure 8. Proposed mechanism of ML and L development. M are present within RPE cells at birth. Unknown processes at the M surface might lead to marginal AF coatings or show focal hotspots of AF. Both scenarios lead to the ML phenotype (I), a combination of M and fluorophores of lipofuscin origin. Simultaneously, ML change their shape from spindle to round. Ongoing reactions form ML granules exhibiting a melanin core and progressive AF coating (II). This ratio (melanin/ fluorophores of lipofuscin origin) finally inverts, with AF material exceeding the enclosed melanin remnants (III). Further remodeling then leads to the formation of pure L granules. Our hypothesis is supported by the high heterogeneity of the ML1–3 group, the decreasing number of M and increasing number of L with age, and the mainly spindle-shaped granules (M and ML) apically and round granules (ML and L) basolaterally and basally (data not shown).

It should be mentioned that the formation of L may be related to melanosomes but is not necessarily related to melanin. Melanosomes are also found within RPE cells in the albino retina,[43] and patients with albinism have highly reflective RPE cells.[44,45] Depending on the mutation, patients with albinism can have defects in melanogenesis or organellogenesis, which are two separate processes.

Number of Autofluorescent Granules per RPE Cell

Our data on the total number of AF granules in the two age groups add valuable knowledge to our understanding of the intracellular changes and granule storage capabilities of RPE cells, as reports on absolute numbers of granules are sparse (Supplementary Table S3).[12,13] Each cell accommodates hundreds of granules, even in young eyes (e.g., 16-year-old donor). Of note, despite this massive granule load, all examined RPE cells looked healthy; that is, the cells exhibited a regular polygonal shape with straight sides and sharp vertices[14] and lacked the granule reorganization seen in AMD.[17,18] Furthermore, epifluorescence and transmission macroscopy of donor eyes before flat-mount preparation revealed no retinal or macular pathologies.[14]

Consistent with our findings on age-related changes, Feeney-Burns et al.[12] reported an increase of L with age in all regions and a decrease of M, whereas the analysis of the fovea by Pollreisz et al.[13] showed only a decrease of M but no change in L. In contrast to the reported increase of ML, we found constant ML numbers. Those discrepancies might have various explanations. First, Pollreisz et al. determined the exact localization of the fovea (as we did in this study), whereas Feeney-Burns et al. estimated the rough localization of the analyzed regions, meaning that the "posterior pole" in the latter study (including macula and optic nerve head) may have contained non-foveal cells, thus reducing the potential comparability to other studies. Second, the study by Feeney-Burns et al.[12] did not examine whole RPE cells but rather single sections, which might have led to some misclassification due to the inability to examine whole granules, especially with regard to the differentiation of L and ML. Third, M are known to be numerous in the apical processes of RPE cells.[46–48] Due to tissue preparation techniques in our study, we cannot reliably guarantee that M within apical processes were imaged using SIM, which might have led to the low number of pure M. However, apical processes contain about 60 melanosomes per RPE cell,[30] meaning that the total number of granules per cell in our study could have been underestimated by about 11% to 19%.

Additionally, melanin-containing granules with only a faint AF coating, possibly caused by inhomogeneous AF of the cytoplasm, could have been falsely classified as ML. This might have led to low M numbers and could explain the discrepancy to high M numbers reported by Feeney-Burns et al.[12] On the other hand, Pollreisz et al.,[13] who used electron microscopy, also reported comparable low numbers of M in cell bodies; however, different imaging techniques, such as electron microscopy (non-fluorescence) versus fluorescence microscopy, might display different phenotypes even if the same granules are imaged.

Implications for Fundus Autofluorescence

Our data on AF-intensity per cell together with the corresponding number and distribution of intracellular granules can inform clinical high-resolution imaging at a new level of precision. New in vivo imaging techniques using adaptive optics modalities are capable of capturing individual RPE cells,[49] and quantification of FAF intensity has also recently been introduced,[50] thus enabling linking clinical data to our histological findings. In the adaptive optics studies, the hypo-AF in en face projection images of RPE cells is sometimes attributed to the non-AF cell nucleus,[49,51] but it should be acknowledged that the central hypo-AF could also represent a high content of melanosomes or melanolipo-

fuscin granules. High-resolution near-infrared autofluorescence imaging could add additional information, as melanin has been reported to contribute to near-infrared autofluorescence signals.[52] In addition, optically dense melanin and melanosomes also play an important role in other imaging modalities such as optical coherence tomography.

Limitations of this study are the restriction of analysis to three retinal locations and the possible loss of RPE apical processes, which might explain the low number of pure M (see above). We also focused on AF emissions at one wavelength (488 nm) and did not address signal sources of emissions at other wavelengths, such as those attributed to melanosomes.[53] A further limitation is that only 10 cells per location were analyzed; however, a mean coefficient of variation of about 25% is in good agreement with results from other RPE granule studies.[13] The manual marking of the granules within a z-stack, though computer assisted, is time consuming; therefore, our upcoming studies will explore artificial intelligence methods as a way to increase sample size. Strengths include systematic imaging at predefined locations of well-preserved RPE flat-mounts with short postmortem time,[14] the use of multiple tissues of two age groups, and the use of a high-resolution imaging technique that enables AF imaging of individual granules. These procedures led to the introduction of a detailed phenotype subclassification of AF granules of human RPE cell bodies. The observed characteristic intracellular distribution, regional differences highlighting the unique biology of the fovea, and age-related changes further highlight the complexity in RPE granule deposition. On the other hand, granule deposition can be simplified if AF signal sources are linked to the overlying photoreceptors.

Nevertheless, the current data are valuable for interpreting clinical FAF images. Ongoing studies should focus on RPE granule accumulation in diseases such as AMD and on spectral properties of individual RPE granules.

Acknowledgments

Supported by the Werner Jackstädt Foundation (TA); by National Institutes of Health grants (1R01EY027948 to TA, CAC; 1R01EY06109 to CAC); by Heidelberg Engineering (CAC); by Genentech/Hoffmann-La Roche (CAC); and by Research to Prevent Blindness and EyeSight Foundation of Alabama institutional support to the University of Alabama Department of Ophthalmology and Visual Sciences (CAC).

Disclosure: **K. Bermond,** None; **C. Wobbe,** None; **I.-S. Tarau,** None; **R. Heintzmann,** None; **J. Hillenkamp,** None; **C.A. Curcio,** MacRegen (I); **K.R. Sloan,** MacRegen (I); **T. Ach,** Novartis (F, R), Roche (C), MacRegen (I)

References

1. Marmorstein AD. The polarity of the retinal pigment epithelium. *Traffic*. 2001;2:867–872.
2. Strauss O. The retinal pigment epithelium in visual function. *Physiol Rev*. 2005;85:845–881.
3. Shi G, Maminishkis A, Banzon T, et al. Control of chemokine gradients by the retinal pigment epithelium. *Invest Ophthalmol Vis Sci*. 2008;49:4620–4630.
4. Feeney L. Lipofuscin and melanin of human retinal pigment epithelium. Fluorescence, enzyme cytochemical, and ultrastructural studies. *Invest Ophthalmol Vis Sci*. 1978;17:583–600.
5. Orlow SJ. Melanosomes are specialized members of the lysosomal lineage of organelles. *J Invest Dermatol*. 1995;105:3–7.
6. Schraermeyer U, Peters S, Thumann G, Kociok N, Heimann K. Melanin granules of retinal pigment epithelium are connected with the lysosomal degradation pathway. *Exp Eye Res*. 1999;68:237–245.
7. Sparrow JR, Gregory-Roberts E, Yamamoto K, et al. The bisretinoids of retinal pigment epithelium. *Prog Retin Eye Res*. 2012;31:121–135.
8. Feeney-Burns L, Berman ER, Rothman H. Lipofuscin of human retinal pigment epithelium. *Am J Ophthalmol*. 1980;90:783–791.
9. Gibbs D, Cideciyan AV, Jacobson SG, Williams DS. Retinal pigment epithelium defects in humans and mice with mutations in myo7a: imaging melanosome-specific autofluorescence. *Invest Ophthalmol Vis Sci*. 2009;50:4386–4393.
10. Taubitz T, Fang Y, Biesemeier A, Julien-Schraermeyer S, Schraermeyer U. Age, lipofuscin and melanin oxidation affect fundus near-infrared autofluorescence. *EBioMedicine*. 2019;48:592–604.
11. Streeten BW. The sudanophilic granules of human retinal pigment epithelium. *Arch Ophthalmol*. 1961;66:391.
12. Feeney-Burns L, Hilderbrand ES, Eldridge S. Aging human RPE: morphometric analysis of macular, equatorial, and peripheral cells. *Invest Ophthalmol Vis Sci*. 1984;25:195–200.
13. Pollreisz A, Messinger JD, Sloan KR, et al. Visualizing melanosomes, lipofuscin, and melanolipofuscin in human retinal pigment epithelium using serial block face scanning electron microscopy. *Exp Eye Res*. 2018;166:131–139.
14. Ach T, Huisingh C, McGwin G, Jr, et al. Quantitative autofluorescence and cell density maps of the human retinal pigment epithelium. *Invest Ophthalmol Vis Sci*. 2014;55:4832–4841.
15. Gliem M, Muller PL, Finger RP, McGuinness MB, Holz FG, Charbel Issa P. Quantitative fundus autofluorescence in early and intermediate age-related macular degeneration. *JAMA Ophthalmol*. 2016;134:817–824.
16. Orellana-Rios J, Yokoyama S, Agee JM, et al. Quantitative fundus autofluorescence in non-neovascular age-related macular degeneration. *Ophthalmic Surg Lasers Imaging Retina*. 2018;49:S34–S42.
17. Ach T, Tolstik E, Messinger JD, Zarubina AV, Heintzmann R, Curcio CA. Lipofuscin redistribution and loss accompanied by cytoskeletal stress in retinal pigment epithelium of eyes with age-related macular degeneration. *Invest Ophthalmol Vis Sci*. 2015;56:3242–3252.
18. Gambril JA, Sloan KR, Swain TA, et al. Quantifying retinal pigment epithelium dysmorphia and loss of histologic autofluorescence in age-related macular degeneration. *Invest Ophthalmol Vis Sci*. 2019;60:2481–2493.
19. Wing GL, Blanchard GC, Weiter JJ. The topography and age relationship of lipofuscin concentration in the retinal pigment epithelium. *Invest Ophthalmol Vis Sci*. 1978;17:601–607.
20. Weiter JJ, Delori FC, Wing GL, Fitch KA. Retinal pigment epithelial lipofuscin and melanin and choroidal melanin in human eyes. *Invest Ophthalmol Vis Sci*. 1986;27:145–152.
21. Østerberg GA. Topography of the layer of rods and cones in the human retina. *Acta Ophthalmol (Copenh)*. 1935;6:1–103.
22. Hughes A. The topography of vision in mammals of contrasting life style: comparative optics and retinal organisation. In: Crescitelli F , ed. *The Visual System in Vertebrates*. Berlin: Springer-Verlag; 1977:613–756.
23. Curcio CA, Sloan KR, Kalina RE, Hendrickson AE. Human photoreceptor topography. *J Comp Neurol*. 1990;292:497–523.

24. Best G, Amberger R, Baddeley D, et al. Structured illumination microscopy of autofluorescent aggregations in human tissue. *Micron*. 2010;42:330–335.
25. Ach T, Best G, Rossberger S, Heintzmann R, Cremer C, Dithmar S. Autofluorescence imaging of human RPE cell granules using structured illumination microscopy. *Br J Ophthalmol*. 2012;96:1141–1144.
26. Curcio CA, Medeiros NE, Millican CL. The alabama age-related macular degeneration grading system for donor eyes. *Invest Ophthalmol Vis Sci*. 1998;39:1085–1096.
27. Polyak SL. *The Retina: The Anatomy and the Histology of the Retina in Man, Ape, and Monkey, Including the Consideration of Visual Functions, the History of Physiological Optics, and the Histological Laboratory Technique*. Chicago, IL: The University of Chicago Press; 1941.
28. Quinn N, Csincsik L, Flynn E, et al. The clinical relevance of visualising the peripheral retina. *Prog Retin Eye Res*. 2019;68:83–109.
29. Schindelin J, Arganda-Carreras I, Frise E, et al. Fiji: an open-source platform for biological-image analysis. *Nat Methods*. 2012;9:676–682.
30. Pollreisz A, Neschi M, Sloan KR, Schmidt-Erfurth U, Curcio CA, Dacey DM. Visualizing melanosomes (M) in apical processes (AP) of human retinal pigment epithelium (RPE) using volumetric serial block-face scanning electron microscopy (SBFSEM). *Invest Ophthalmol Vis Sci*. 2018;59:1506.
31. Hogan MJ, Alvarado JA, Weddell JE. *Histology of the Human Eye: An Atlas and Textbook*. Philadelphia, PA: Saunders. 1971.
32. Starnes AC, Huisingh C, McGwin G, Jr, et al. Multi-nucleate retinal pigment epithelium cells of the human macula exhibit a characteristic and highly specific distribution. *Vis Neurosci*. 2016;33:e001.
33. Wang JS, Kefalov VJ. The cone-specific visual cycle. *Prog Retin Eye Res*. 2011;30:115–128.
34. Streeten BW. Development of the human retinal pigment epithelium and the posterior segment. *Arch Ophthalmol*. 1969;81:383–394.
35. Abramov I, Gordon J, Hendrickson A, Hainline L, Dobson V, Labossiere E. The retina of the newborn human infant. *Science*. 1982;217:265–267.
36. Hendrickson AE, Yuodelis C. The morphological development of the human fovea. *Ophthalmology*. 1984;91:603–612.
37. Yuodelis C, Hendrickson A. A qualitative and quantitative analysis of the human fovea during development. *Vision Res*. 1986;26:847–855.
38. Hendrickson A, Possin D, Vajzovic L, Toth CA. Histologic development of the human fovea from midgestation to maturity. *Am J Ophthalmol*. 2012;154:767–778.e2.
39. Quazi F, Molday RS. ATP-binding cassette transporter ABCA4 and chemical isomerization protect photoreceptor cells from the toxic accumulation of excess 11-*cis*-retinal. *Proc Natl Acad Sci U S A*. 2014;111:5024–5029.
40. Boyer NP, Higbee D, Currin MB, et al. Lipofuscin and *N*-retinylidene-*N*-retinylethanolamine (A2E) accumulate in retinal pigment epithelium in absence of light exposure: their origin is 11-*cis*-retinal. *J Biol Chem*. 2012;287:22276–22286.
41. Dontsov AE, Sakina NL, Ostrovsky MA. Loss of melanin by eye retinal pigment epithelium cells is associated with its oxidative destruction in melanolipofuscin granules. *Biochemistry (Mosc)*. 2017;82:916–924.
42. Biesemeier A, Schraermeyer U, Eibl O. Chemical composition of melanosomes, lipofuscin and melanolipofuscin granules of human RPE tissues. *Exp Eye Res*. 2011;93:29–39.
43. Cortese K, Giordano F, Surace EM, et al. The ocular albinism type 1 (oa1) gene controls melanosome maturation and size. *Invest Ophthalmol Vis Sci*. 2005;46:4358–4364.
44. Wilk MA, McAllister JT, Cooper RF, et al. Relationship between foveal cone specialization and pit morphology in albinism. *Invest Ophthalmol Vis Sci*. 2014;55:4186–4198.
45. Schutze C, Ritter M, Blum R, et al. Retinal pigment epithelium findings in patients with albinism using wide-field polarization-sensitive optical coherence tomography. *Retina*. 2014;34:2208–2217.
46. Zhang QX, Lu RW, Messinger JD, Curcio CA, Guarcello V, Yao XC. In vivo optical coherence tomography of light-driven melanosome translocation in retinal pigment epithelium. *Sci Rep*. 2013;3:2644.
47. Kim IT, Choi JB. Melanosomes of retinal pigment epithelium–distribution, shape, and acid phosphatase activity. *Korean J Ophthalmol*. 1998;12:85–91.
48. Steinberg RH, Wood I, Hogan MJ. Pigment epithelial ensheathment and phagocytosis of extrafoveal cones in human retina. *Philos Trans R Soc Lond B Biol Sci*. 1977;277:459–474.
49. Granger CE, Yang Q, Song H, et al. Human retinal pigment epithelium: In vivo cell morphometry, multispectral autofluorescence, and relationship to cone mosaic. *Invest Ophthalmol Vis Sci*. 2018;59:5705–5716.
50. Delori F, Greenberg JP, Woods RL, et al. Quantitative measurements of autofluorescence with the scanning laser ophthalmoscope. *Invest Ophthalmol Vis Sci*. 2011;52:9379–9390.
51. Tam J, Liu J, Dubra A, Fariss R. In vivo imaging of the human retinal pigment epithelial mosaic using adaptive optics enhanced indocyanine green ophthalmoscopy. *Invest Ophthalmol Vis Sci*. 2016;57:4376–4384.
52. Lapierre-Landry M, Carroll J, Skala MC. Imaging retinal melanin: a review of current technologies. *J Biol Eng*. 2018;12:29.
53. Keilhauer CN, Delori FC. Near-infrared autofluorescence imaging of the fundus: visualization of ocular melanin. *Invest Ophthalmol Vis Sci*. 2006;47:3556–3564.

Supplementary Material

Supplementary Video. Three-dimensional z-stack video of an RPE cell. The RPE cell was imaged from apical to basal using structured illumination microscopy. Step size = 100 nm. RPE cell was from the near-periphery. Donor was an 83-year-old female.

Investigative Ophthalmology & Visual Science